Malaysian Journal of Chemistry, 2007, Vol. 9, No. 1, 029 - 039

Flow Analysis in Falling Coaxial Cylinder Viscometer for Polymer Melts

K. K. Chee*
Department of Chemistry, University of Malaya, 50603 Kuala Lumpur, Malaysia
* Present correspondence address: C-16-6, PV3, 3 Jalan Melati Utama 3,
Taman Melati Utama, Setapak, 53100 Kuala Lumpur, Malaysia.

Abstract : Basically, the falling coaxial cylinder viscometer (FCCV) consists of a stationary cylinder containing the polymer melt, and an inner cylinder or rod driven vertically into the fluid by a constant force. The laminar flow of the fluid through the cylindrical annulus is described by the equation of motion. An important feature of this treatment is the resort of the power law model, instead of the Newtonian model used in the early study, to obtain the velocity gradient of the flow. Apparently, both the shear stress and shear rate are susceptible to the power law index, n, which is observed to vary from 0.52 to 1.05 in the present study. This gives rise to the discrepancies between the flow curves from different rod geometries and driving forces. As such, the raw data have been appropriately dealt with by considering the end effects inherent to the apparatus. In this work, the true flow curves of a commercial polystyrene (PS) and a high-density polyethylene (PE) at shear rates ranging from 0.10 to 0.40 s^{-1} are reported. They are found to obey the power law equation and Cross equation. The latter offers the zero shear viscosity with values reported for the two polymers at 186 ^{o}C. For the sake of comparison, the other relevant data are derived from the reliable sources. The difference between the melt flow data based on the power law and Newtonian models is also highlighted. It is concluded that the present rigorous flow analysis in FCCV would result in the congruous and dependable low shear viscosity data for the polymer melts.

Abstrak : Pada asasnya, viskometer FCCV (kependekan 'Falling Coaxial Cylinder Viscometer') terdiri daripada suatu silinder tetap yang mengandungi lebur polimer dikaji, dan suatu silinder atau rod dalaman yang ditekan secara menegak supaya memasuki cecair tersebut dengan suatu daya tertentu. Aliran laminar cecair yang melalui tempat berbentuk cincin antara kedua-dua silinder itu boleh digambarkan persamaan gerakan. Suatu ciri penting mengenai pengendalikan ini adalah penggunaan model hukum kuasa yang menggantikan model Newtonian terpakai dahulu, supaya memperoleli cerunan halaju aliran cecair. Nampaknya, kedua-dua ricihan tegasan dan ricihan kadar seterusnya bergantung kepada indek hukum kuasa, n, yang didapati berubah dari 0.52 ke 1.05. Akibatnya, lengkung-lengkung aliran dihasilkan daripada beberapa geometri rod dan daya gunaan, memang berbeza bagi suatu sample polimer. Dengan demikian, data-data kasar harus dikendalikan sewajarnya dengan menimbangkan kesan-kesan hujung yang bersedia ada dalam alat ini. Dalam kajian ini, lengkung-lengkung aliran betul yang meliputi ricihan kadar daripada 0.10 ke 0.40 s^{-1} bagi suatu polistirena (PS) komersil dan suatu polietilena (PE) ketumpatan tinggi, telah dilaporkan. Terdapat bahawa mereka mematuhi persamaan hukum kuasa dan persamaan Cross. Tambahan pula, persamaan Cross mendatangkan nilai-nilai kelikatan ricihan sifar bagi kedua-kedua polimer tersebut pada 186 ^{o}C. Untuk perbandingan selanjutnya, data-data berkenaan pula diterbitkan daripada punca-punca lain. Perbezaan antara data-data aliran lebur polimer berdasarksan model hukum kuasa dan model Newtonian juga ditegaskan. Adalah disimpulkan bahawa analisis aliran tepat FCCV kali ini menghasilkan data-data kelikatan ricihan rendah yang konsistan dan dipercayai bagi lebur-lebur polimer.

Received : 23.07.07; accepted : 04.01.08

Introduction

The coefficient of viscosity or simply viscosity,η, may be derived from the flow data by taking the ratio of the shear stress and shear rate. For the polymer melts, the measurements of η are usually performed by the capillary extrusion viscometer, which can deliver the η values in the order of 10^5 Pa.s over a range of shear rates from about 1 s^{-1} to 1.2 x 10^4 s^{-1} [1]. This rheological information is of considerable importance to understanding and solving problems encountered in polymer processing. A somewhat lower shear rate region may be accessible by the rotational viscometry. Recently, a centrifugal ball viscometer has been developed to measure directly the zero shear viscosity, η_o, of polytetrafluoroethylene melts by Chu et al. [2], who have determined, among others, a considerably high η_o=5.2 x 10^9 Pa.s at 380 ^{o}C and low shear rate below

10^{-6} s^{-1}. These low shear viscosity data have been shown to be useful for characterizing a molecular weight average of the polymer.

The falling coaxial cylinder viscometer (FCCV) is a novel, simple, and inexpensive apparatus. It has produced the flow curves (plotting shear stress against shear rate) of polymer melts at low shear rate regions covering 0.07 to 0.50 s^{-1} approximately. The details of this technique are described elsewhere [3-7]. However, the previous working equations are derived based on the Newtonian fluids. Although this early version of flow analysis has been validated with the result of a standard fluid of known η_o [7], its generality is unwarranted. The main objective of the present work is to rectify this situation by applying the power law model as a mathematical analogy of the viscous behavior of polymer melts. To this end, we have to address the problem of experimental discrepancies between the different rods and driving weights. In addition, the flow curves obtained by means of the power law and Newtonian models are compared to confirm that the present elegant analysis is indeed unparalleled, reliable and versatile.

Flow analysis

The essential parts of the apparatus are a closed-end cylinder with inner radius r_a, and a rod of smaller radius r_i. The former containing the polymer melt is fixed. Whereas the inner rod is driven vertically into the viscous fluid by a deadweight, W, with a rate of falling, V_i, which gradually decreases with increasing time, t, and immersion length, L. In fact, the excess pressure, p, at the level of the bottom of the rod forces the fluid below upwards with a velocity profile across the concentric cylindrical annulus, $v_z(r)$, as illustrated in Figure 1, which also defines the other physical parameters [3].

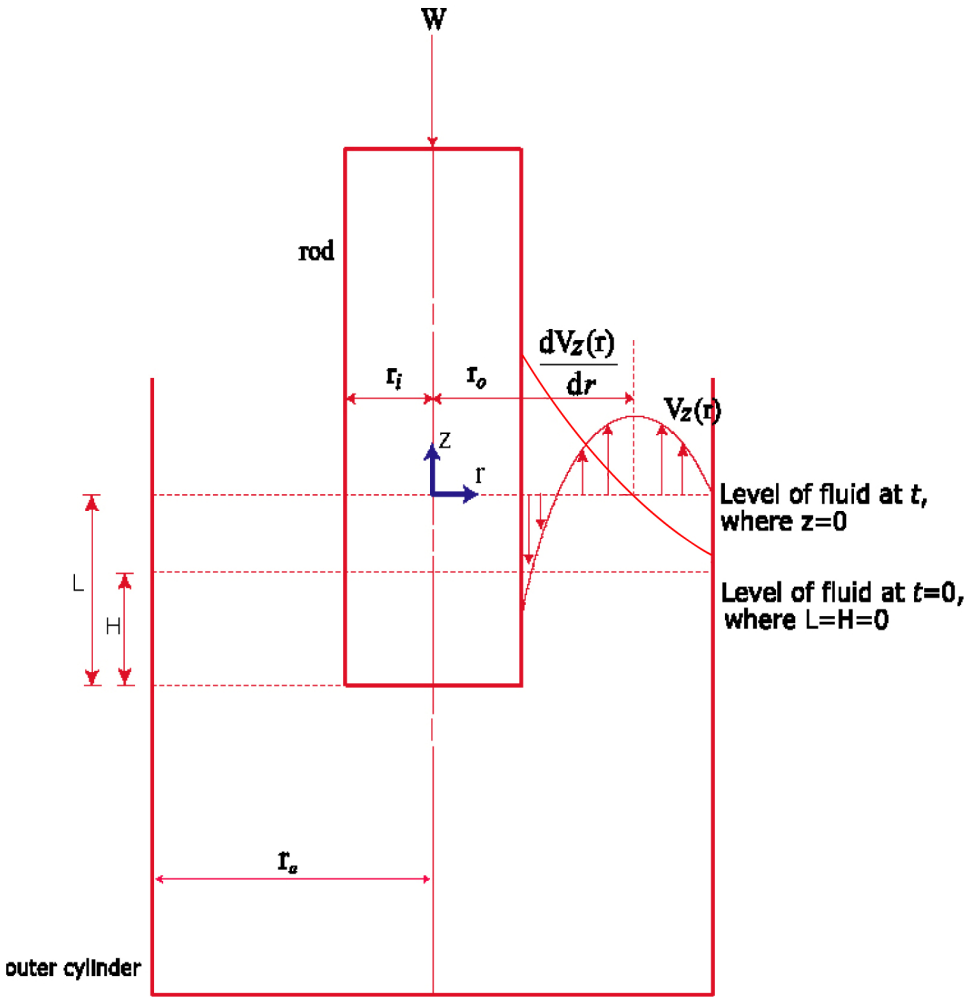

Figure 1 : Flow Parameters

It is crucial to assume that the flow of the fluid through the annulus is laminar, so that it may be readily analyzed by the equation of motion [8,9]. In cylindrical coordinates (z, r, θ), the z-component of the equation is given by

$$\rho (\partial v_z / \partial t + v_r \partial v_z / \partial r + v_\theta \partial v_z / r \partial \theta + v_z \partial v_z / \partial z) = - \partial P / \partial z + (\partial r\tau_{rz} / r \partial r + \partial \tau_{\theta z} / r \partial \theta + \partial \tau_{zz} / \partial z) + \rho g_z \quad (1)$$

where ρ is the density of the fluid, v_i is the i-component of the local fluid velocity **v**, P is the fluid pressure, τ_{iz} is the z-directed shear stress on the plane perpendicular to the axis defined by the first subscript, i.e. i-axis, and g_z is the z-component of the gravitational acceleration **g**, with i= r, θ, z.

For an incompressible liquid, the partial derivative $\partial v_z / \partial z$ in eq. (1) vanishes according to the equation of continuity. The other terms on the left hand side of the equation are either zero or negligibly small, and so is the gravity component term on the right hand side. Under the present conditions, we further drop $\partial\tau_{\theta z} / \partial\theta$ and $\partial\tau_{zz} / \partial z$ reducing eq. (1) to

$$dr\tau_{rz} / r\, dr = dP / dz \quad (2)$$

By considering the pressures between z=-L, and 0, we obtain dP / dz=-p/L. Then integrating with respect to r in eq. (2) results in

$$\tau_{rz} = - r\, p / 2L + A / r \quad (3)$$

where A is an integration constant.

The power law equation takes the form

$$\tau_{rz} = k_1 | dv_z/dr |^{n-1} dv_z/dr \quad (4)$$

where k_1 and n are the model constants [1], with the latter specifically known as the power law index. Eqs. (3) and (4) lead to

$$dv_z(r)/dr = (p / 2k_1L)^{1+m} | r_o^2 / r - r |^m (r_o^2 / r - r) \quad (5)$$

where the velocity profile, $v_z(r)$, replaces v_z hereafter, and r_o is defined by the maximum point of $v_z(r)$ as

$$[dv_z(r)/dr](r_o) = o \quad (5a)$$

and $$m = 1 / n - 1 \quad (5b)$$

Hereafter, the derivative in eq. (5) is designated by $[dv_z(r)/dr]_L$ for $r \le r_o$, and $[dv_z(r)/dr]_R$ for $r \ge r_o$. The former is given by

$$[dv_z(r)/dr]_L = (r_o p / 2k_1L)^{1+m} (s / \sqrt{(1 - s)})^{1+m} \quad (6)$$

where $s = 1 - (r/r_o)^2$ (6a)

Likewise, the latter is expressed by

$$[dv_z(r)/dr]_R = - (r_o p / 2k_1L)^{1+m} (u / \sqrt{(1 + u)})^{1+m} \quad (7)$$

where $u = (r/r_o)^2 - 1$ (7a)

Since the rate of liquid volume displaced by the downward rod is equated to the rate of volume forced up into the annular region, we have

$$\pi r_i^2 V_i = \int_{r_i}^{r_a} 2 \pi r v_z (r) dr \quad (8)$$

Assuming no slippage at the polymer-metal interfaces, the boundary conditions $v_z(r_i) = - V_i$, and $v_z(r_a) = 0$ are introduced into eq. (8) to yield

$$\int_{r_i}^{r_a} r^2 [dv_z(r)/dr] dr = o \quad (9)$$

This definite integral is divided into two parts for the ensuing analysis

$$\int_{r_i}^{r_o} r^2 [dv_z(r)/dr]_L\, dr + \int_{r_o}^{r_a} r^2 [dv_z(r)/dr]_R\, dr = 0 \quad (10)$$

Eq. (10) is converted to a handy form by changing the variable r to s and u via eqs. (6)-(7a). In order to carry out the relevant integrations analytically, it is necessary to expand the factors $(1 - s)^{-m/2}$ and $(1 + u)^{-m/2}$, which appear in the transformed form of eq. (10), in power series and neglect altogether the terms higher than the third powers of s and u. On the basis of the boundary conditions $s(r_o) = u(r_o)$, and setting $s_i = 1- (r_i / r_o)^2$, $u_a = (r_a / r_o)^2 - 1$, eq. (10) finally results in

$$f_2 - (m/2)f_3 + (m/2)(1 + m/2)f_4/2! - (m/2)(1 + m/2)(2 + m/2)f_5/3! = 0 \quad (11)$$

where $f_l = [u_a^{l+m} - (-1)^l s_i^{l+m}] / (l + m)$; $l = 2,3,4,5$ (11a)

Eq. (11) is used to solve for the characteristic radius r_o, which plays a critical role in this study.

When $r = r_o$, we have $\tau_{rz}(r_o) = 0$, as inferred from eq. (4). Then eq. (3) leads to the shear stress at $r = r_i$, i.e. $\tau_{rz}(r_i)$, hereafter designated by

$$\tau_i = r_o^2 p\, s_i / 2Lr_i \quad (12)$$

which is related to the shear rate at r_i, $[dv_z(r)/dr]_i$, by the power law equation, i.e. an alternative form of eq. (4) for positive shear rate

$$\tau_i = k_1 [dv_z(r)/dr]_i^n \quad (13)$$

By virtue of the boundary conditions pertaining to eq. (9), the velocity of the rod may be expressed by

$$-V_i = \int_{r_a}^{r_o} [dv_z(r)/dr]_R \, dr - \int_{r_i}^{r_o} [dv_z(r)/dr]_L \, dr \quad (14)$$

Eqs. (6) and (7) inserted into eq. (14), and the integrations are performed by means of power series expansion as above. The resulting equation is combined with eqs. (11)-(13) to achieve

$$[dv_z(r)/dr]_i = K V_i \quad (15)$$

where $K = 2s_i^{1+m} / r_i(1 - s_i)^{m/2}[f_3 - (1+m/2)f_4 + (1+m/2)(2+m/2)f_5/2]$ (15a)

In practice, V_i is determined by taking the readings of the position of the falling rod, h, and the corresponding time t continuously. If the rod position registered at t=0 is h_o, the distance traveled by the rod over an interval of time t is $H=|h - h_o|$. Hence, we have

$$V_i = dH/dt \quad (16)$$

The applied force on the rod is opposed by the hydrostatic force and the viscous drag of the fluid. As a result, the net force responsible for the downward movement of the rod in a depth L is

$$W(dV_i/dt) = Wg - 2\pi r_i L\tau_i - \pi r_i^2 p \quad (17)$$

where g is the gravitational acceleration constant. In this connection, the buoyancy correction on W is insignificant and ignored, and so is the term on the left hand side since the acceleration dV_i/dt is much smaller than g [5,7]. Eqs. (12) and (17) are combined to give

$$\tau_i = Wgs_i / 2\pi r_i L \quad (18)$$

for a sufficiently large L.

The volume of liquid displaced by the falling rod over a given duration is forced up around the rod giving $\pi r_i^2 H = \pi(r_a^2 - r_i^2)(L - H)$, which can be arranged to

$$L = \alpha H \quad (19)$$

where $\alpha = r_a^2 / (r_a^2 - r_i^2)$ (19a)

Perhaps, one of the interesting findings of the present investigation is a single power law relationship between the distance H, and the time, t

$$H^\delta = \beta t \quad (20)$$

where δ and β are the empirical constants. Hence, eq. (16) becomes

$$V_i = \beta / \delta H^{\delta-1} \quad (21)$$

which is experimentally accessible. Inserting eqs. (19) into (18) indicates $\tau_i \propto H^{-1}$, whereas eqs. (21) into (15) demonstrates $[dv_z(r)/dr]_i \propto H^{-(\delta-1)}$. This means the derivatives $d\ln\tau_i / d\ln H = -1$, and $d\ln([dv_z(r)/dr]_i)/d\ln H = -(\delta-1)$. It follows that the power law index, n, is given by

$$\begin{aligned} n &= d\ln\tau_i / d\ln([dv_z(r)/dr]_i) \\ &= (d\ln\tau_i / d\ln H) / (d\ln([dv_z(r)/dr]_i)/d\ln H) \\ &= 1 / (\delta-1) \end{aligned} \quad (22)$$

Hence, eq. (5b) becomes

$$m = \delta - 2 \quad (23)$$

which may be used in conjunction with eqs. (15), (15a) and (21) to calculate $[dv_z(r)/dr]_i$ at a given H.

Combining eqs. (12), and (18) yields the pressure in the melt,

$$p = Wg / \pi r_o^2 \quad (24)$$

which is intimately related to m.

One of the important assumptions made in the foregoing analysis is the laminar flow. However, this does not seem to hold true around the square end of the rod where there is a converging stream into the annular region. Another non-unidirectional flow occurs immediately below the bottom of the rod itself. All these end effects produce internal frictional losses, which can be dealt with in terms of the effective depth designated by L + e. Herein the parameter e is the apparent incremental depth arising from the foregoing effects. By analogy to the treatment of end effects in capillary viscometers [10], we replace L in eq. (17) by L + e to obtain

$$L + e = p_i r_i(1 - p/p_i) / 2\tau_I \quad (25)$$

where $p_i = Wg / \pi r_i^2$ (25a)

The factor p_i is just a pressure exerting on the static surface of a polymer without causing any viscous flow. Accordingly, the pressures p_i and p (eq. (24)) may be visualized as the amount of energy per unit volume fully transported to the melt by the action of the weight W, and that retained in the melt after the rod movement, respectively. This means that the factor $(1- p/p_i)$ in eq. (25) physically represents the fraction of energy loss due to the viscous dissipation. Incidentally, the foregoing factor is equal to s_i. By intuition, we assume that the end correction factor e is directly proportional to r_i and $(1-p/p_i)$ concomitantly, to obtain the effective shear stress from eq. (25)

$$\tau_i = p_i / 2(L/r_i s_i + \lambda) \qquad (26)$$

where λ is a constant of proportionality defined by

$$e = \lambda r_i s_i \qquad (26a)$$

Hence, eqs. (15) and (26) give the true shear rate and shear stress at the wall of the falling rod respectively, based on the power law model characterized by eq. (23).

Results and discussion

Primary data for this study are extracted from references [3,4,11]. They are listed in Tables 1-3.

Table 1 includes the values of the radius r_i and the instrument constant for seven rods. According to eq. (20), a double logarithmic plot of H against t would result in a straight line, from which the constants δ and β are derived for an applied weight, W. In order to estimate the true τ_i, it is necessary to deal with the end effects. To this end, the foregoing exercise is extended to a selection of rods and loads. The overall results on β and δ are displayed in Table 2 for the PS, and Table 3 for the PE at 186 ^oC. It is noted that the present studies embrace the pseudoplastic ($\delta>2$) and dilatant ($\delta<2$) flow behavior of the polymer melts. However, these δ values are fairly close, particularly for the PS sample. In contrast, the factor β increases consistently with increasing W and decreasing r_i, effecting the low rates of deformation all along. This means that the velocity profiles across the annular gap characterized by the power law index n (eq.(22)) varying from 0.67 to 1.04 for the PS, and 0.53 to 1.05 for the PE, do not seem to change significantly under the low shear conditions with FCCV.

Eqs. (15), (21) and (26) show that both $[dv_z(r)/dr]_i$ and τ_i decrease with increasing distance H. This means that in theory one would be able to construct the extended flow curves for the systems of interest based on the data cited in Tables 1-3. However, this is not practiced for the following reasons. At the early stage of the rod movement, the resulting $[dv_z(r)/dr]_i$ and τ_i are grossly erroneous due to the prominent relative error in H. On the other hand, prolong shearing of a polymer melt till high depth may have disrupted the rheological structural units of flow. In addition, all polymer melts are susceptible to chain scissions on excessive heating at elevated temperatures. As such, the present study merely considers the optimum H values varying from 0.21 to 2.1 cm for the PS, and 0.23 to 3.1 cm for the PE. In any event, the duration of the rod movement did not exceed 30 minutes.

There was a concern about the implication of locating imprecisely the initial position of the rod designated by h_o^* [5]. In order to address this problem the following analysis is considered. Eq. (20) should have been written in terms of h_o^* as

$$\left| h - h_o^* \right|^{\delta} = \beta t \qquad (27)$$

Eq. (27) can be recast to

$$\left| \pm H + \Delta h_o \right|^{\delta} = \beta t \qquad (28)$$

where $\Delta h_o = h_o - h_o^*$ (28a)

Table 1: Rod Radii and Instrument Constant

Rod No.	r_i/cm	$\alpha^{(a)}$
S1	0.6744	3.4308
S2	0.6492	2.9117
S3	0.5721	2.0403
S4	0.4699	1.5243
E1	0.7074	4.5363
E2	0.5500	1.8912
E3	0.4750	1.5420

(a) The radius of the barrel is 0.8012 cm.

As the second and higher power terms of $\Delta h_o/H$ are inappreciable, eq. (28) can be rearranged and simplified to

$$\ln H \pm \Delta h_o/H = (\ln\beta + \ln t) / \delta \qquad (29)$$

Clearly, eq. (29) is equivalent to eq. (20) when the measured H is much larger than $|\Delta h_o|$. This means that an exact knowledge of the initial rod position is not crucial in determining the constants δ and β provided that a plot of lnH against lnt is linear. However, deviation from the foregoing linearity does occur when H is as short as or comparable to $|\Delta h_o|$. In contrast, no such undesirable events have been encountered for the sufficiently high H values, thus ruling out practically the adverse effects of over-heating and excessive shearing in the polymer melts being studied.

If m = 0, the definite integrals in eq. (10) may be evaluated analytically to yield $u_a = s_i$ and eventually

$$r_o = [(r_a^2 + r_i^2) / 2]^{1/2} \qquad (30)$$

However, eq. (11) instead should be used for the same purpose when m is not an integer. The Newton's method [12] is available for solving eq. (11) using the iterative formula

$$x_{n+1} = x_n - F(x_n) / F'(x_n) \qquad (31)$$

where the function F is defined by the left hand side of eq. (11), and $F'=\partial F/\partial x$, with the argument $x=r_o$. Eq. (30) conveniently offers the first approximation (i.e. n=1) of x (i.e. $x_1=r_o$), which ensures rapid convergence to a root of $F(r_o)=0$.The results on r_o thus obtained are listed in Tables 2-3, which also include the values of K (eq. (15a). A total of eleven sets of the relevant data are displayed for the PS (Table 2) using various falling rods and loading weights. Table 3 presents a collection of data for the PE.

Eqs. (15) and (26) are now invoked to evaluate shear rate and shear stress as follows. The ranges of the H to be studied are first identified by referring to the linear portions of the lnH – lnt plots. Eqs. (15) and (21) may be used to calculate the shear rate from H and vice versa. For each of the experiments shown in Tables 2-3, it is imperative to calculate the p_i (eq. (25a)). Figure 2 shows the linear relationships between p_i and $L/r_i s_i$ at 0.15 s^{-1} and 0.40 s^{-1}, and the

Table 2: Raw Data and Related Instrument Parameters for the Polystyrene (PS) at 186 ^oC

Rod No.	W/g	$\beta x10^3/cm^{\delta}/s$	δ	r_o/cm	K/cm^{-1}
S1	1306.4	0.746	2.20	0.74018	161.9
	1806.4	1.19	2.27	0.74007	166.0
	2383.8	1.59	2.25	0.74010	164.8
S2	1768.2	3.08	2.50	0.72804	125.8
	2375.1	3.93	2.30	0.72845	117.4
S3	607.3	3.80	1.97	0.69633	46.19
	807.3	5.56	2.15	0.69525	49.86
	1006.2	7.14	2.11	0.69548	49.05
	1282.7	10.5	2.24	0.69475	51.70
S4	294.8	8.53	1.96	0.65734	22.99
	494.8	14.5	2.02	0.65651	23.67

Table 3: Raw Data and Related Instrument Parameters for the Polyethylene (PE) at 186 ^oC

Rod No.	W/g	$\beta x10^3/cm^{\delta}/s$	δ	r_o/cm	K/cm^{-1}
E1	1183.5	0.267	2.48	0.75536	323.0
	2643.0	0.860	2.77	0.75516	352.7
	4135.5	1.68	2.83	0.75513	358.8
	8158.0	6.15	2.90	0.75509	366.0
E2	271.5	5.27	2.18	0.68588	42.34
	471.5	10.6	2.27	0.68529	43.92
	671.5	16.2	2.32	0.68497	44.79
E3	268.8	14.2	1.95	0.65929	23.52
	368.8	17.8	1.95	0.65929	23.52
	568.8	47.0	2.18	0.65636	26.21

maximum and minimum spreads of L/r_is_i for the PS at 186 ^oC. Herein, two straight lines are drawn to represent the linear equations resulting from the linear-least-squares (LLS) treatments of the data. The intercept on the ordinate, I, and the gradient, G, of each of the straight lines would result in the effective shear stress τ_i (=G/2), and the end-correction term λ (=I/G), according to eq.(26). It follows that the foregoing LLS calculations finally lead to the uncertainties in τ_i and λ at a fixed shear rate. This algorithm of data reduction is followed throughout the present work for any values of m including m=0.

Previous flow analysis in FCCV relies on the Newtonian model characterized by m=0, at which eqs. (15) and (18) are readily reduced to their corresponding expressions cited in reference [3]. This one-parameter model is reexamined herein because of its simplicity and possibility of rendering an alternative to the present method.

On the basis of the information in Tables 2-3, the foregoing methods developed for the FCCV provide the results on τ_i and λ at various shear rates as shown in Table 4 for the PS and PE at 186 ^oC. The reliability of the power law method is demonstrated by the standard deviation in τ_i, which is equal to 0.35 x 10^3 Pa for the PS, and 0.05 x 10^3 Pa for the PE. Clearly, the low shear stress measurements for the PE are more precise. This may be partially attributed to the considerable difference in the spreads of the variable L/r_is_i involved in the end correction plots (like Figure 2), between the two polymers. The PE experiments cover a wider range of L/r_is_i for a given shear rate, and therefore result in the more dependable τ_i statistically [16]. This observation would definitely have a direct impact on choosing the appropriate experimental variables such as the sizes of rods and loading weights, for achieving the best results with the present technique.

The degree of end correction expressed in terms of the ratio e/L (=$\lambda/L/r_is_i$) is found to vary from about 0.12 to 2.0 based on the 19 data points included in Figure 2. Hence, the energy losses due to end effects are indeed significant, particularly at high τ_I or low H.

Table 4 also shows that the power law and Newtonian models produce two distinct sets of shear rate-shear stress data for each of the two polymer melts. Specifically, the former results in τ_i consistently lower than the latter at a given shear rate by about 10% and 20% for the PS and PE respectively. This means that by no means the present analysis for the FCCV can be substituted by the simpler version developed earlier [3,4]. In addition, the negative λ values registered for the PE at low shear rates are rather irrational. The foregoing observations indicate the inadequacies of the Newtonian model for the present systems. Hence, it is ignored altogether in the ensuing pursuits.

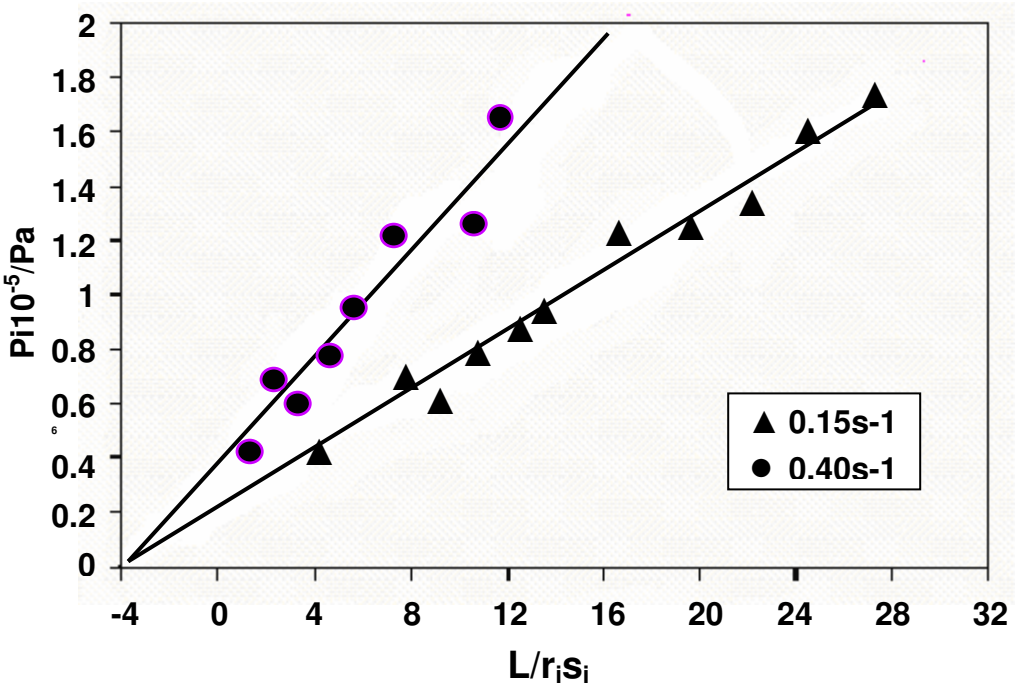

Figure 2 : Typical plots of p_i against L/r_is_i for the polystyrene at 186^oC. The shear rates are 0.15s^{-1} and 0.40s^{-1}.

Table 4 : Low Shear Flow Behavior of Polystyrene (PS) and Polyethylene (PE) at 186 ^{o}C

Polymer	$[dv_z(r)/dr]_i$ /s^{-1}	Power Law Model (i.e. m=δ-2)		Newtonian Model (i.e. m=0)	
		τ_i x 10^{-3}/Pa	λ	τ_i x 10^{-3}/Pa	λ
PS	0.10	2.19±0.14[(a)]	2.4±1.6[(b)]	2.42±0.15[(a)]	2.0±1.5[(b)]
	0.15	2.86±0.19	2.9±1.3	3.12±0.15	3.0±0.9
	0.20	3.45±0.24	3.0±1.2	3.77±0.21	3.0±0.8
	0.30	4.54±0.38	2.7±1.1	4.90±0.33	2.9±0.8
	0.40	5.20±0.59	3.0±1.2	5.80±0.57	2.8±1.1
PE	0.10	1.48±0.04[(a)]	0.3±0.8[(b)]	1.80±0.03[(a)]	-1.5±0.4[(b)]
	0.15	1.96±0.06	0.6±0.9	2.34±0.07	-0.6±0.7
	0.20	2.33±0.04	1.0±0.7	2.81±0.06	0.1±0.7
	0.30	2.85±0.05	1.8±0.6	3.39±0.06	1.0±0.5
	0.40	3.28±0.07	2.4±0.6	3.91±0.07	1.5±0.5

(a) uncertainty in τ_i; (b) uncertainty in λ.

Figure 3 shows the linear plots of $\ln\tau_i$ against $\ln([dv_z(r)/dr]_i)$ for the two thermoplastics. The LLS treatments of the straight lines show that they do conform to the power law equation (i.e. eq. (13)) of the forms

$$\tau_i = 9.50 \times 10^3 [dv_z(r)/dr]_i^{0.63} \quad (32)$$

$$\tau_i = 5.64 \times 10^3 [dv_z(r)/dr]_i^{0.57} \quad (33)$$

over $0.10 \leq [dv_z(r)/dr]_i\ /s^{-1} \leq 0.40$, for the PS and PE respectively.

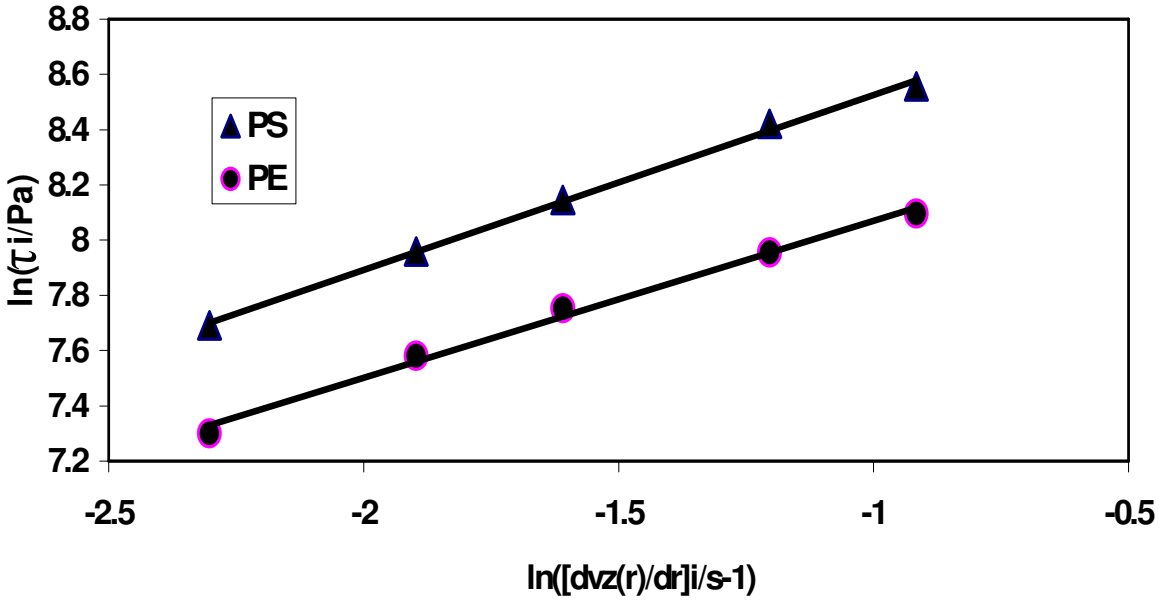

Figure 3 : Double logarithmic plots of τ_i against $[dv_z(r)/dr]_i$, for the polystyrene(PS), and polyethylene(PE) at 186 ^{o}C, based on the power law equation.

Figure 4 is constructed according to the Cross equation [13,14], plotting the fluidity (equal to the reciprocal of η) against $[dv_z(r)/dr]_i^{2/3}$. Two straight lines are drawn to fit the data satisfactorily for the PS and PE, respectively leading to

$$1/\eta = 2.59 \times 10^{-5} + 9.27 \times 10^{-5} [dv_z(r)/dr]_i^{2/3} \quad (34)$$

$$1/\eta = 2.97 \times 10^{-5} + 1.69 \times 10^{-4} [dv_z(r)/dr]_i^{2/3} \quad (35)$$

over $0.10 \leq [dv_z(r)/dr]_i / s^{-1} \leq 0.40$. Taking the reciprocal of the intercept at $[dv_z(r)/dr]_i = 0$ yields the Newtonian (zero shear) viscosity, $\eta_o = 3.9 \times 10^4$ Pa.s from eq. (34) and 3.4×10^4 Pa.s from eq. (35). This particular procedure for determining η_o will be recalled whenever the situation arises.

The high shear flow behavior of the foregoing polymer melts has been studied by the compressed gas operated capillary rheometry and a biconical rheometry [3,11]. For the shear rate ranging from 15.0 to 100 s^{-1}, the capillary extrusion data from the PS at 186 ^oC are found to obey

$$\tau_i = 1.20 \times 10^4 [dv_z(r)/dr]_i^{0.34} \quad (36)$$

While the combined data of the last two high shear rheometers for the PE at 186 ^oC are satisfactorily reproduced by

$$\tau_i = 1.28 \times 10^4 [dv_z(r)/dr]_i^{0.50} \quad (37)$$

over a wider range of $[dv_z(r)/dr]_i$ from 1.0 to 10 s^{-1}.

The fluidity of a power law fluid is related to shear rate by $1/\eta \propto [dv_z(r)/dr]_i^{1-n}$, indicating that the η_o is inaccessible by the Cross equation if n=1/3. Since the power law index, n, in eq. (36) is close to this figure, the associated Cross equation results in the η_o approximately 2.5 times higher than that just cited for the PS above. Despite of this, the literature values of η_o reported for the polystyrene samples of about the same molecular weight distributions as ours vary from 2.6×10^4 to 5.0×10^4 Pa.s [4]. Notably, Hyun and Karam [15] have quoted $\eta_o = 3.5 \times 10^4$ Pa.s, which is lower than our result reported for the PS by less than 10%. Unlike eq. (36), eq. (37) leads to $\eta_o = 2.9 \times 10^4$ Pa.s, which is compatible with our estimate for the PE via the Cross equation.

We have noted that our melt flow data predict the η_o values, which compare favorably with those derived from other reliable sources. Unfortunately, attempt to match them directly with the other dependable flow curves at the shear rates overlapping with ours is out of the question, because the latter information is not available as far as the two polymers of interest are concerned.

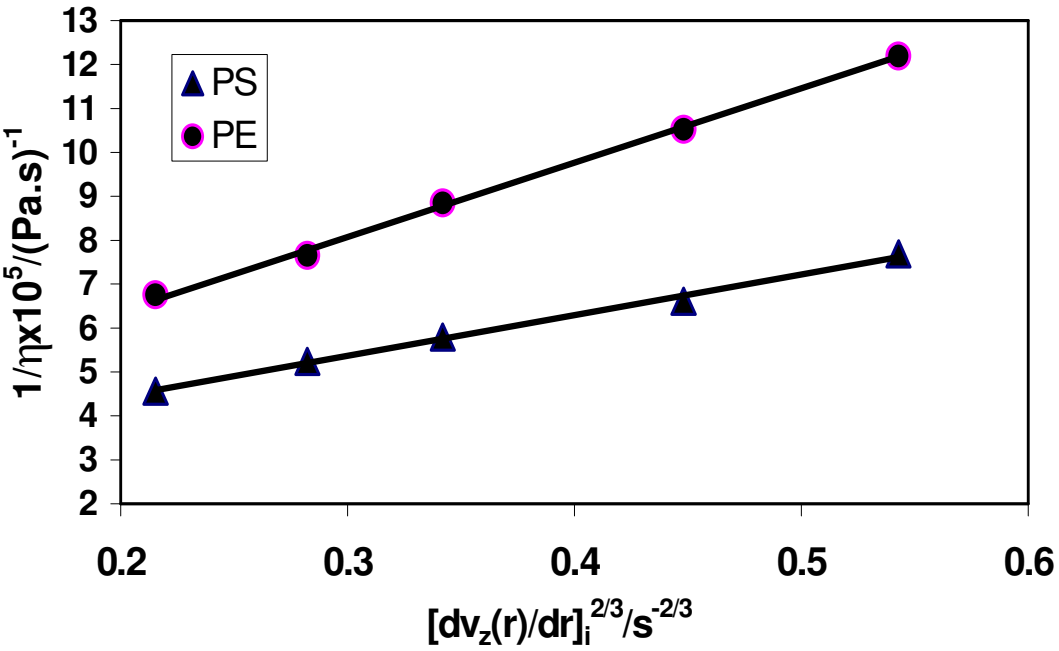

Figure 4 : Linear plots of $1/\eta$ against $[dv_z(r)/dr]_i^{2/3}$, for the polystyrene(PS), and polyethylene(PE) at 186 ^oC, based on the Cross equation.

Although the foregoing analysis applies exclusively to a low shear viscometer, it may be readily modified to suit the high shear rate studies. In fact a novel device has been described, in which the descending rod is driven mechanically at a set speed and the responded force gradient,dW/dH, is recorded electronically all along, particularly when the rod has reached the steady state. The method is based on the Newtonian model covering the shear rates ranging from about 2.0 to 100 s^{-1} for polymer melts [17]. However, the present findings strongly suggest that this rheometry needs to be reconsidered in terms of a two-parameter model. This study is underway.

Conclusion

The present analysis using the power law model has rectified the imperfectness of the previous study on the flow pattern in FCCV. Apparently, this approach leads to the lower shear stress flow curves consistently compared with the method of Newton's law of viscosity. Another significant finding of this rigorous consideration is the importance of the end effects to eq. (18), which is then amended to a useful form (i.e. eq. (26)). As our data cover only a limited range of shear rate, they are satisfactorily represented by both the power law and Cross equations. The latter is graphically translated into a straight line, which is able to extract the η_o with accuracy by means of short-range extrapolation. For the PS and PE samples studied at 186 ^oC, the η_o values are found to be 3.9 x 10^4 and 3.4 x 10^4 Pa.s, respectively.

Acknowledgement

The author thanks Chee Keguan for his technical assistance in preparing this manuscript.

Nomenclature

A integration constant (eq.(3))
e apparent incremental depth
f_l parameter (eq.(11a)); l=2,3,4,5
F a function (eq.(31))
F' a derivative of F (eq.(31))
$\mathbf{g}$ gravitational acceleration
g gravitational acceleration constant
g_z z-component of $\mathbf{g}$
G gradient
h rod position at t
h_o practical rod position at t=0
h_o^* true rod position at t=0
H distance traveled by the rod over time t
I intercept
k_l constant of power law model (eq.(4))
K constant (eq.(15a))
L immersion depth
m power index (eq.(5b))
n power law index (eq.(4))
p excess pressure
p_i static pressure (eq.(25a))
P fluid pressure
r radial position (Figure 1)
r_a radius of outer cylinder
r_i radius of rod
r_o distance r defined by the maximum $v_z(r_o)$ (Figure (1))
s parameter eq(6a))
s_i s at r_i
t time
$\mathbf{v}$ local fluid velocity
v_i i-component of **v;** i=z, r, θ
v_z velocity profile (Figure 1)
V_i velocity of falling rod
u parameter (eq.(7a))
u_a u at r_a
W loading weight
x_n parameter (eq.(31))
x_{n+1} parameter (eq.(31))
z z-component of cylindrical coordinates (Figure 1)
α instrument constant (eq.(19a))
β empirical constant (eq.(20))
δ empirical constant (eq.(20))
η viscosity
η_o zero shear viscosity
θ a component of cylindrical coordinates
ρ density of fluid
λ proportionality constant (eq.(26a))
τ_i shear stress τ_{rz} at r_i
τ_{iz} z-directed shear stress
τ_{rz} shear stress τ_{iz} when i=r

References

1. J.R. Van Wager, J.W. Lyons, K.Y. Kim, and R.E. Colwell (1966) "Viscosity and Flow Measurement", *Interscince, New York*, **4**.
2. B. Chu, and L. Kung (1998) *Macromolecules*, **28**, 2723.
3. K.K. Chee, and A. Rudin (1970*) Can. J. Chem., Eng*., **48**, 362.
4. K.K. Chee, and A. Rudin (1971) *Polym. Eng. Sci.,* **11**, 35.
5. K. Sato, A. Rudin, and K.K. Chee (1972) *Can. J. Chem., Eng.,* **50**, 576.
6. K.K. Chee, and A. Rudin(1976) *Can. J. Chem., Eng.,* **54**, 129.
7. K.K. Chee, K. Sato, and A. Rudin (1976*) J. Appl. Polym. Sci*., **20**, 1467.
8. R.B. Bird, W.E. Stewart, and E.N. Lightfoot (1960) "Transport Phenomena", *John Wiley, New York*, **3**.
9. J.A. Brydson (1970) "Flow Properties of Polymer Melts", *Butterworth, London*, **7**.
10. E.B. Bagley (1957) *J. Appl. Physics*, **28**, 624.
11. K.K. Chee (1972) Ph.D. Thesis, University of Waterloo, Waterloo, Ontario, Canada

12. F. Scheid (1968) "Schaum's Outline Series: Numerical Analysis", *McGraw Hill, New York*, **25**.
13. M.M. Cross (1966) *Eur. Polym., J.,* **2**, 299.
14. M.M. Cross (1965) *J. Colloid Interface Sci*., **20**, 471.
15. K.S. Hyun, and H.J. Karam (1965) *Trans Soc. Rheol.,* **13**, 335.
16. N.R. Draper and H. Smith (1981) "Applied Regression Analysis", *John Wiley, and Sons, New York*, **1**,
17. K.K. Chee, and A. Rudin (1977) *Rheol. Acta*., **16**, 635.